Rev. Adv. Mater. Sci. 44 (2016) 361-369

FABRICATION OF ALUMINUM-GRAPHENE AND METAL-CERAMIC NANOCOMPOSITES. A SELECTIVE REVIEW

V.G. Konakov[1,2], O.Yu. Kurapova[1,2], I.V. Lomakin[2], I.Yu. Archakov[1,3,4], E.N. Solovyeva[4], and I.A. Ovid'ko[1,2,3]

[1]Research Laboratory for Mechanics of New Nanomaterials,
Peter the Great St. Petersburg Polytechnic University, Polytechnicheskaya 29, St.Petersburg 195251, Russia
[2]Saint Petersburg State University, 7/9 Universitetskaya nab., St. Petersburg, 199034 Russia
[3]Institute for Problems of Mechanical Engineering, Bolshoi pr. VO 61, St. Petersburg, 199178, Russia
[4]Glass and Ceramics Ltd., 9 Linia V.O., 20, St. Petersburg, 199004, Russia

Received: May 10, 2016

Abstract. This paper addresses nanoengineering approaches developed to synthesize metal (Al)-graphene and metal (Al, Ni, Ti, nano-Ti)–ceramic (yttrium stabilized zirconia) nanocomposites. Approaches are considered which provide "wafer-coating" and "bulk composite" geometries of the synthesized nanocomposites. With the experimental data on their microstructure, phase composition, thermal, and mechanical characteristics, we discuss the effects of nanoinclusions on the properties exhibited by these nanocomposites. Optimized synthesis technologies are suggested which allow one to fabricate metal-ceramic and metal-graphene nanocomposites with desired structures and properties.

1. INTRODUCTION

Metal-matrix nanocomposites represent advanced materials that are highly attractive for a wide range of structural and functional applications. Indeed, modification of the microstructure of metallic materials by nanoscale inclusions can effectively enhance and control various properties of these materials. In recent years, a rapidly growing attention has been devoted to graphene (Gr) sheets and nanoplatelets that exhibit the unique electronic, mechanical, and thermal properties [1-4] and thereby are of utmost interest for use as fillers in metal-matrix composites. In particular, with superior mechanical properties (strength ≈ 130 GPa, Young modulus ≈ 1 TPa) of graphene [5], its sheets and nanoplatelets serve as excellent strengthening inclusions in metal-matrix composites [6].

Among metal-graphene nanocomposites, Al-Gr composites have attracted a special attention due to low weight of aluminum, coupled with its high strength and good ductility. Following Refs. [7-10], insertion of graphene nanoinclusions into Al matrix significantly increases both hardness and fracture strength. At the same time, plasticity of Al-Gr composites is rather poor. For instance, in tensile test [7], a nanocomposite consisting of Al-matrix reinforced by 0.3 wt.% graphene showed both tensile strength of 256 MPa and 13% elongation which are by 62% higher and nearly 2 times lower than the strength (154 MPa) and elongation (27%) of pure (unreinforced) Al, respectively.

At the same time, there are several technical problems in synthesis of Al-Gr composites. First, conventional and relatively cheap powder metallurgy

Corresponding author: V.G. Konakov, e-mail: glasscer@yandex.ru

(PM) approach is hardly applicable in the synthesis under consideration, because pure Al cannot be compacted without lubricants like fatty metal salts, amide and/or polyethylene waxes, graphite mix with mineral oil, etc. However, use of these lubricants in the synthesis procedure usually results in such negative effects as structural non-homogeneities and crack generation in final composites. Sometimes, fracture of PM-processed specimens is observed in even their green or annealed states. Another problem is to eliminate lubricants from final composites and prevent their chemical reactions with Al matrix. Several approaches were suggested to solve this problem. They represent modified versions of PM technique, including heat pretreatment or hot pressing, in which case the modified approaches are rather complicated. In addition, defect accumulation and aluminum carbide formation in composite specimens after their heat pretreatment or hot pressing were reported; see, e.g., [11]. In the context discussed, there is large interest in searching for new methods for fabrication of Al-graphene nanocomposites with enhanced mechanical characteristics especially ductility. The first main aim of this paper is to elaborate a new approach to fabricate Al-graphene nanocomposites with enhanced plasticity (section 3.1).

In parallel with metal-graphene nanocomposites, metal-ceramic nanocomposites represent perspective metal-matrix composite materials for current and future high technologies. In this case, nanoceramics (i.e., ceramics that are synthesized from nanoscale precursor powders and possess some specific characteristics due to this synthesis method) are exploited as nanoinclusions in various metal matrixes. In particular, nanoscale particles of yttrium stabilized zirconia (YSZ, Y_2O_3-ZrO_2) in the form of cubic or tetragonal solid solution serve as such ceramic nanoinclusions in advanced metal-ceramic nanocomposites.

Among metal-YSZ composites, Ti-YSZ nanocomposites are of utmost interest, because titanium and its alloys are traditional biocompatible materials widely utilized in fabrication of medical implants and prostheses. These materials possess required chemical inertness and sufficient biocompatibility, but their strength characteristics are definitely worth being improved for medical applications. In order to enhance strength of implants made of titanium, recently, it has been suggested to use nanostructured titanium in medical engineering [12]. This idea is based on the fact that nanostructured metals typically exhibit strength and hardness which are 2-10 times higher than those of their conventional coarse-grained polycrystalline counterparts; see, e.g., [13,14].

YSZ coatings [15-17] are considered as coatings of a new type for titanium due to their excellent biocompatibility and high mechanical properties. In doing so, zirconia modifications with high symmetry (i.e. tetragonal and cubic) are preferred. Zirconia-coated Ti demonstrates enhanced working characteristics, as compared to those exhibited by pure Ti; see, e.g., [18].

However, the deposition of zirconia-based, and, in particular, YSZ, coatings on titanium is a formidable challenge, because of low adhesion of such ceramic coatings to Ti surface. More than that, in the situation where YSZ ceramic coatings are deposited on nanostructured titanium (nano Ti), some additional difficulties, say, thermal stability of the nanostructure in Ti [19], come into play. The third main aim of this paper is to present recently developed developed new approaches addressing deposition of YSZ coatings on conventional and nanostructured Ti wafers (section 3.2).

In parallel with metal-ceramic nanocomposites having wafer-coating geometry, bulk metal-ceramic nanocomposites, i.e. metal-matrix composites modified by nanoceramics, are also of large interest. Such a modification gives a possibility to increase thermal and chemical stability of composite materials as well as tune and control their mechanical and other properties. In particular, Ni-YSZ nanocomposites represent very promising materials for high temperature technologies (metallurgy, spacecrafts, etc.) due to rather high melting temperature of pure Ni (1453 °C). The use of YSZ nanoceramic inclusions as fillers in Ni matrix is prosperous, since melting temperature of YSZ is very high, so that the increase in thermal resistivity of Ni-YSZ composite is expected, as compared to pure Ni. Besides, enhancement of the mechanical properties could be an additional benefit from insertion of YSZ nanoinclusions into Ni matrix. The use of YSZ-Ni composites with the prevailing YSZ content (that is, the case of ceramic matrix modified by metallic inclusions) is described in Ref. [20,21]. Such composite materials serve as basic ones for anodes of high-temperature fuel cells. At the same time, research efforts focused on Ni matrix composites modified with YSZ ceramics are very limited. This motivates both fabrication of such Ni-YSZ nanocomposites and examination of their properties. Similarly, with excellent characteristics of aluminum and YSZ ceramics, it is logical to expect

Table 1. Al-Gr compositions under study.

Al-ASD +3wt.%Gr			Al-ASD +5wt.%Gr			Al-PA4 +1wt.%Gr			Al-PA4 +3wt.%Gr		
annealing temperature, °C											
400	450	500	400	450	500	400	450	500	400	450	500
IA	IB	IC	IIA	IIB	IIC	IIIA	IIIB	IIIC	IVA	IVB	IVC

that Al-YSZ nanocomposites can show high thermal stability and enhanced mechanical properties. The fourth main aim of this paper is to present recently developed approaches focused on fabrication of bulk Ni-matrix composites containing YSZ nanoinclusions (section 3.3).

2. EXPERIMENTAL

In our research efforts addressing chemical engineering approaches to synthesis of metal-graphene and metal-ceramic nanocomposites, the following experimental techniques were utilized.

Particle-size distributions (PSD) were measured using Horiba LA 950 PSD analyzer. Phase compositions were characterized by XRD technique (SHIMADZU XRD-6000, Cu-Kα with λ = 1.54 Å at room temperature). Optical microscopy (OM) (OM, Olympus bx51), SEM (Zeiss Supra V-55), and TEM (Jeol JEM-1230) were exploited in order to characterize the microstructure of materials. SEM analysis was performed at the Center for Geo-Environmental Research and Modeling (GEOMODEL) of Research park of St.Petersburg State University.

In addition, for the same aims, we used electron backscattering diffraction technique (EBSD, TESCAN MIRA 3LMH FEG scanning electron microscope equipped with an EBSD analyzer "CHANNEL 5"). As to details, a rectangular greed with 50 nm scan step was utilized with standard clean-up procedures with a grain tolerance angle of 5° and a minimal grain size of 3 pixels. Grain sizes were measured from the data on distances between high-angle grain boundaries specified by misorientation angles > 15°.

Chemical compositions were analyzed using EDX and X-ray fluorescence data (INCA Microanalysis systems). Raman spectroscopy (RS, SENTERRA, T64000, excitation wave length 488 nm, gate voltage 40 V) was exploited to identify graphene in metal-graphene composites. Nanotest (Micro Materials Co.) was used to perform nanoindentation tests. Compression tests were carried out utilizing SHIMADZU AG X-Plus (50 kN at 5 $\cdot 10^{-4}$ sec^{-1} deformation rate).

3. RESULTS AND DISCUSSION

3.1. Bulk aluminum-graphene nanocomposites

This section presents a new approach developed for fabrication of bulk Al-Gr nanocomposites. This approach represents a modified version of the general PM method, exploiting deformation-induced graphite-to-graphene transformations realized via micromechanical splitting. In the framework of the suggested approach, graphite and/or graphene inclusions that are present in initial aluminum powder mixes and then in compacted composite structures serve as very special lubricants effectively solving the problem of Al compactification discussed in Section 1. Commercial fine and coarse Al powders with average particle sizes of 7 and ≈30 μm, respectively, were utilized as initial metallic components of composites. (In Russian classification, these fine- and coarse-grained Al powders are called Al-ASD and Al-PA-4, respectively). Also, a meshing of Al powders was performed in order to exclude fractions with a grain size larger than 40 μm. Commercial thermally expanded graphite (TEG) was used as another initial component, namely a source for graphene nanoplatelets produced in graphite-to-graphene transformations induced by ball mill treatment.

Al-TEG mixtures with various (1-5 wt.%) TEG contents were grinded in a planetary mill (Pulverisette 6) at 450 rpm for 3 hours. As it has been shown earlier [23], such a milling process (coupled to mechanical activation) gives rise to the TEG-to-graphene transformation occurring through micromechanical splitting. XRD, TEM, and RS data convincingly confirm this transformation. In particular, according to RS data, graphene in the synthesized composites is present in a form of nanosheets/nanoplatelets with a number of graphene layers varying from 1 to 4. Four final compositions of the synthesized composites were chosen for their further examination; see Table 1.

Al-Gr powders after the ball milling treatment can be easily compacted by cold pressing (with pres-

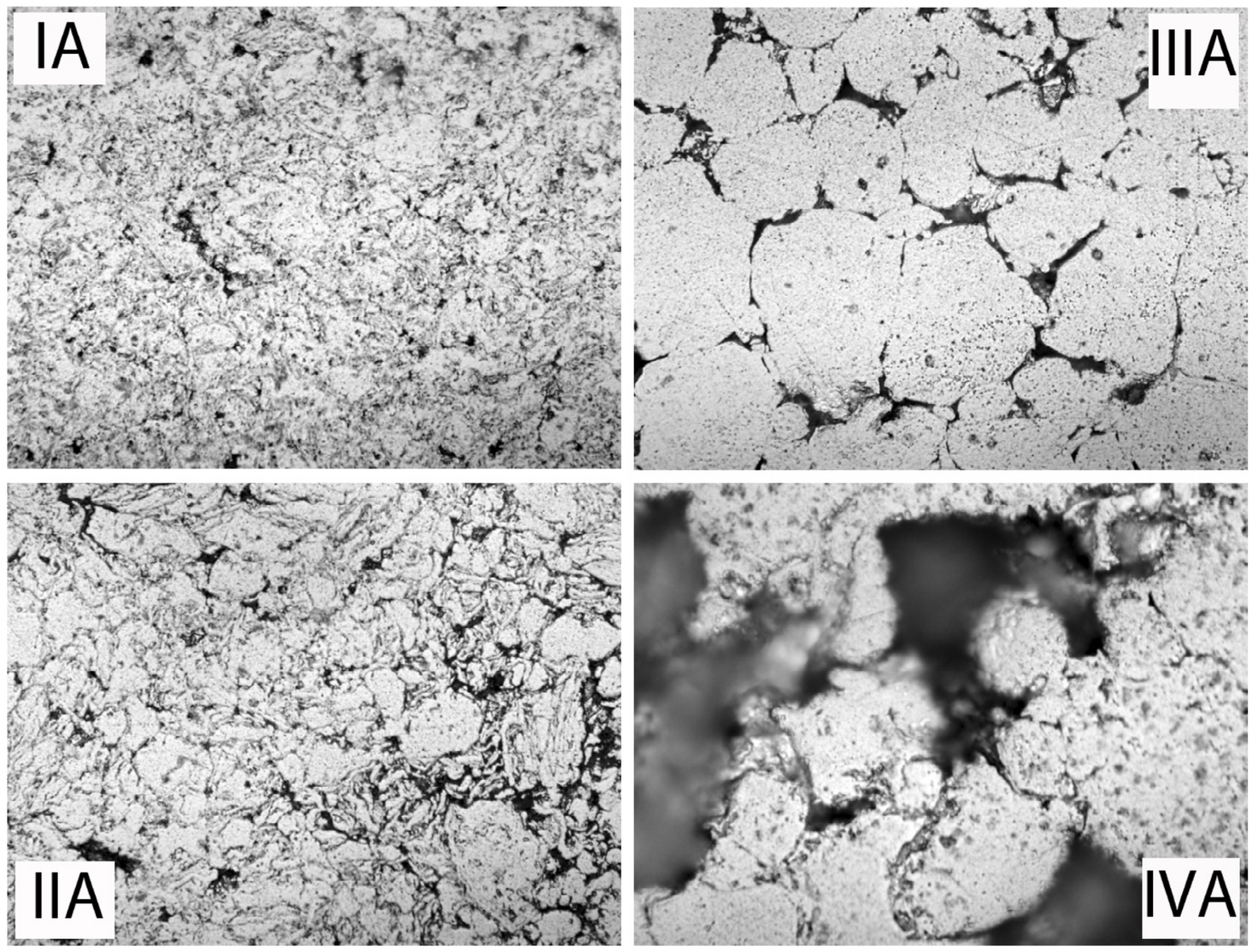

Fig. 1. Surface of the Al-Gr nanocomposites – optical microscopy data.

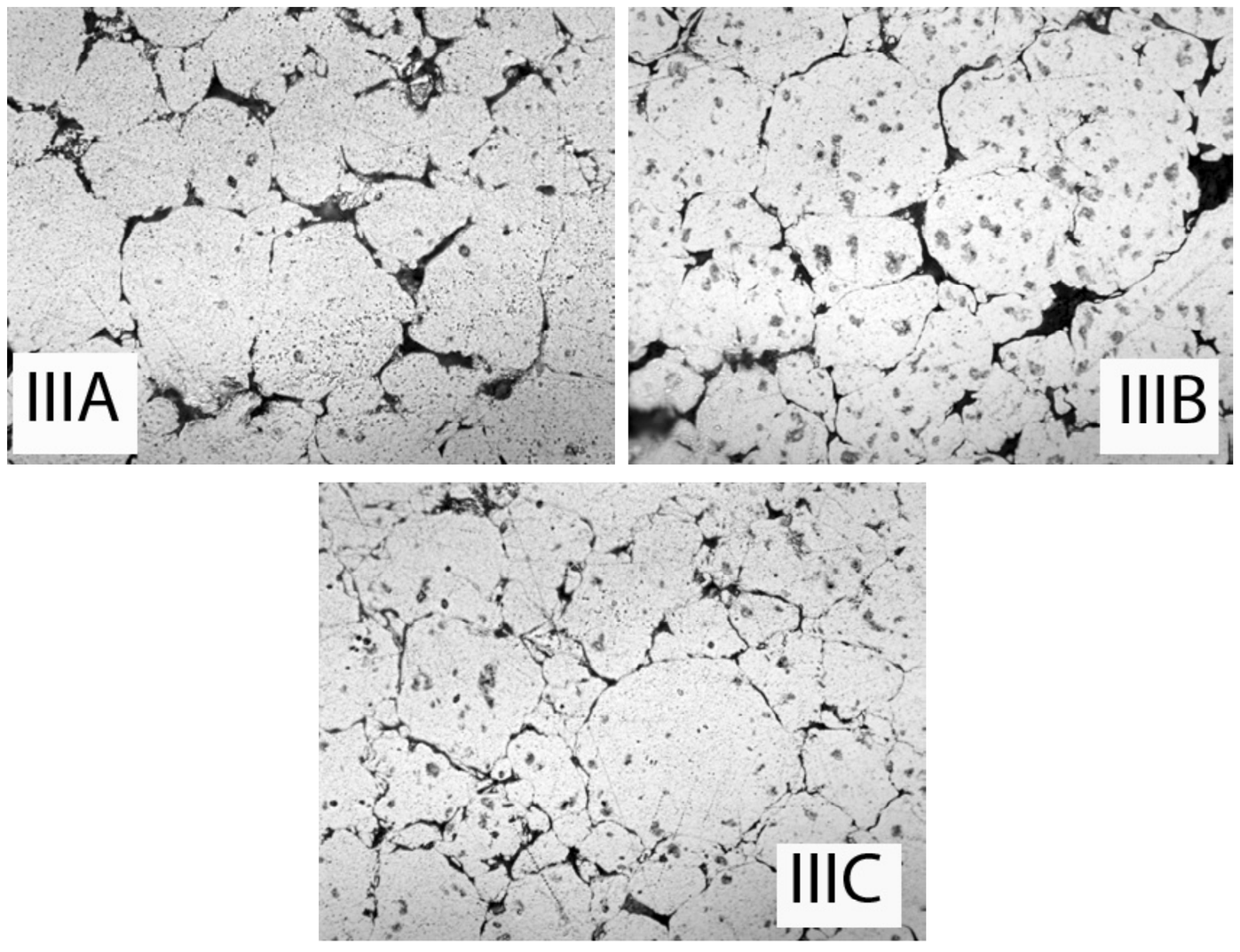

Fig. 2. The effect of the annealing temperature on the Al-Gr nanocomposites microstructure – optical microscopy data.

sure of 2125 kg/cm^2 at room temperature) [24]. Within the suggested approach, the compacted specimens were annealed in a vacuum furnace during 30 min. With thermogravimetry data, annealing temperatures of 400, 450, and 500 °C were chosen. Note that all these temperatures are lower than the melting point of pure aluminum.

Fig. 1 presents the OM data for specimens with various Gr contents and degrees of Al powder dispersity after thermal annealing at 400 °C. As it follows from this figure, the surface uniformity is quite well in the case of fine Al-ASD powder with minimal Gr content (specimen IA, Fig. 1a), while the surface of IVA composite fabricated from coarse-grained Al-PA4 powder is very rough. So, one can conclude that the uniformity of Al-Gr nanocomposite microstructure decreases with rising the average particle size of Al powder and/or Gr content. In particular, use of coarse Al powder with a large amount of graphene nanoplatelets results in the structure

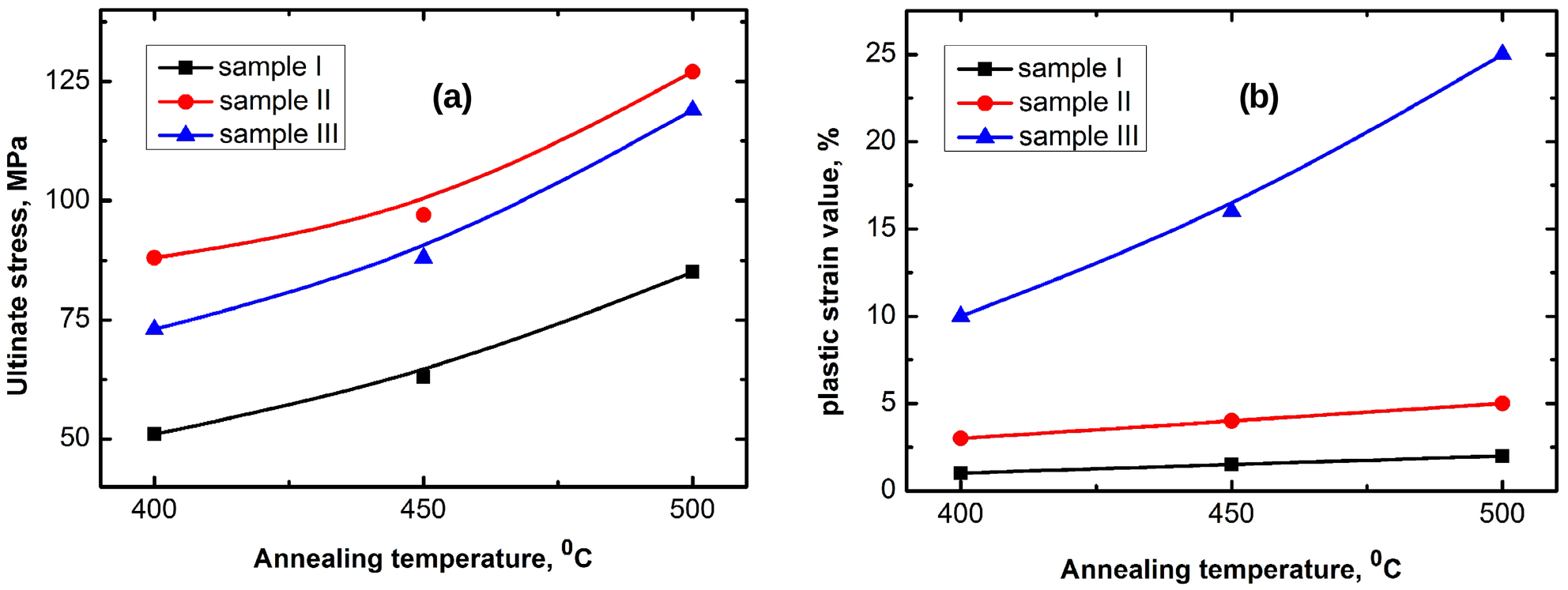

Fig. 3. Mechanical properties of Al-Gr nanocomposites.

containing many pores with relatively high linear dimensions.

The effect of annealing temperature is demonstrated in Fig. 2 for specimen III (Al-PA4 with 1 wt.% of Gr). As it follows from this figure, an increase in the annealing temperature makes the nanocomposite microstructure to be more uniform. Indeed, many cracks are observed at the surface of the specimen produced via annealing at 400 °C (IIIA). The significant decrease in both the number of cracks and their linear dimensions is observed in specimen IIIB, annealed at 450 °C, whereas the structural uniformity of specimen IIIC annealed at 500 °C is quite fine.

Also, Fig. 1 shows that the structure of the specimen IV is fairly non-uniform. This drawback manifests itself in preparation of specimens for mechanical tests. To prepare such specimens, cylinders with ∅ 4.5 mm and 9 mm in high were cut from nanocomposites I-IV by electric discharge cutting technique. However, it was impossible to process the specimen IV, since the composite specimen was significantly fractured at the cutting procedure. As a corollary, mechanical tests were finally performed for only specimens I, II, and III. The test results obtained using SHIMADZU AG X-Plus machine are presented in Fig. 3 showing both ultimate stress (σ_T) and plastic strain-to-failure (ε_{pl}) for these specimens. Note that the tests were carried out in two directions: along and normal to the direction of specimen compaction. It was shown that the results of both tests agree with each other within the limits of experimental error.

As it follows from Fig. 3, both the ultimate stress and plastic strain-to-failure increase when the annealing temperature grows. This trend correlates well with the annealing temperature effect on the microstructure uniformity of Al-Gr nanocomposites; see our previous discussion of data presented in Fig. 2. More precisely, with increase in annealing temperature, the number of fabrication-produced flaws like cracks (that can initiate fast brittle fracture at low external stress levels) decreases in a composite specimen so that its ultimate strength and ductility increase (Fig. 3).

In particular, the specimen IIIC fabricated from coarse Al powder with 1 wt.% Gr at annealing temperature of 500 °C demonstrates remarkable ductility characterized by the plastic strain ≈25%. This high value of the plastic strain is close to that (≈27% [7]) exhibited by pure Al and much higher than plastic strain degrees inherent in both Al-matrix composites fabricated by modified PM methods [7-10] and other Al-Gr composite specimens (IA, IB, …, IIIB; see Table 1) fabricated in this study. The excellent plastic properties of the Al-Gr composite IIIC as compared to Al-composites produced by other research groups [7-10] are logically attributed to high structural uniformity (with a low number or even absence of fabrication-produced flaws like cracks that initiate fast fracture processes) achieved in our new fabrication approach exploiting the role of few-layer graphene nanoplatelets as special plastic elements. (In these nanoplatelets, plastic flow occurs through enhanced relative shear between graphene layers having weak layer-layer binding by Van der Waals forces). Enhanced plasticity of the specimen IIIC, as compared to other Al-Gr composite specimens (Table 1) fabricated in this study, is related to its structure consisting of coarse grains (originated from comparatively large powder particles involved in the compactification process) that are conventionally more ductile than fine grains.

We now discuss the effects exerted by Al powder dispersity and Gr content on the ultimate strength of Al-Gr composites. In general, since graphene

Table 2. Estimates of the average agglomeration size in the $9Y_2O$-$91ZrO_2$ precursor powders.

Salt concentration, M	0.01	0.05	0.1
BET estimates for average agglomerate size, nm	44	57	89

nanoplatelets serve as effective obstacles for lattice dislocations mediating plastic flow in metals, the ultimate strength should tend to grow with rising the graphene content. Also, high-angle grain boundaries are formed at contacting free surfaces of powder particles during their compactification process, and these grain boundaries hamper lattice dislocation slip in Al-Gr composites. As a corollary, composite specimens fabricated from fine Al powders should tend to have larger strength values, as compared to composites synthesized from coarse Al powders. The discussed effects of Al powder dispersity and Gr content manifests itself in the fact that the maximal values of the ultimate strength σ_T are observed for the specimen II produced from fine Al powder containing 5 wt.% Gr (Fig. 3a). However, there is a discrepancy between the discussed effects and the experimentally documented fact that the specimen II fabricated from coarse Al with low Gr content of 1% showed higher σ_T values than the specimen I (Al-ASD, 3 wt.% Gr). In order to elucidate the origin of the discrepancy in question, further research in this area is needed. Currently, such examinations are in progress.

3.2. Ti-YSZ nanocomposites with wafer-coating geometry

In general, magnetron sputtering seems to be an optimal technique for deposition of ceramic coatings on titanium. This approach provides high purity of the deposited coating along with the high strength of wafer-coating binding. In addition, magnetron sputtered coatings usually possess high surface and bulk uniformity. So, it was quite reasonable to exploit such a technique to deposit YSZ nanoceramics on nanostructured titanium.

The key problem in realization of this idea is in fabrication of the magnetron target. Such a target should be made of cubic zirconia-based solid solution in order to obtain cubic modification of the coating which seems to be most effective in achieving the desired structure of Ti-YSZ composites. Also, a target should be free of additions conventionally used to form YSZ ceramics, namely organic additions like polymethylmethacrylate or inorganic ones like Na- or Ca-silicates).

In the framework of our approach, YSZ ceramic system containing 9 mol.%Y_2O_3 was used for the magnetron target, In this case, the precursor powders for the ceramics were synthesized by sol-gel reverse precipitation method. $ZrO(NO_3)_2$'"$2H_2O$, $Y_2O_3(NO_3)_3$'"$6H_2O$, and, for target with titanium oxide, $TiOSO_4$'"$2H_2$ along with aqueous ammonia solution were utilized as initial reagents. 0.01-0.1M salt solutions in water were prepared and thoroughly mixed in the required proportions, and 0.1M ammonia solution was utilized as a precipitator. The prepared salt solutions mixture was placed into this ammonia solution so that the volume fraction of ammonia solution was 10 times higher than the fraction of salt solution mixture. Salt solutions were added at a rate of 1-2 mL/min at constant stirring. The process occurred in an ice bath at temperature 0 °C, and pH was kept at 9-10. The obtained hydroxide mixtures was cleaned from water, NH_4OH, and NH_4NO_3 by centrifugation. After that, the obtained gel was washed by distilled water using the Buchner funnel. Low-temperature drying (Labronco dryer) was exploited. Such a drying gives an opportunity to produce precursor powders with a low average particle size. Moreover, low agglomeration level was reported for such powders.

The produced precursor powders were ball milled using Pulverisette 6 (agate mortar with a set of agate balls, 350 rpm for 2 hours). The further steps of the preparation of precursor powders were annealing at 550 °C and ultrasound treatment in order to minimize agglomeration of particles. Nanosized fraction of the powder was separated using "Gefest-2" air separator. As a result, powders with an average

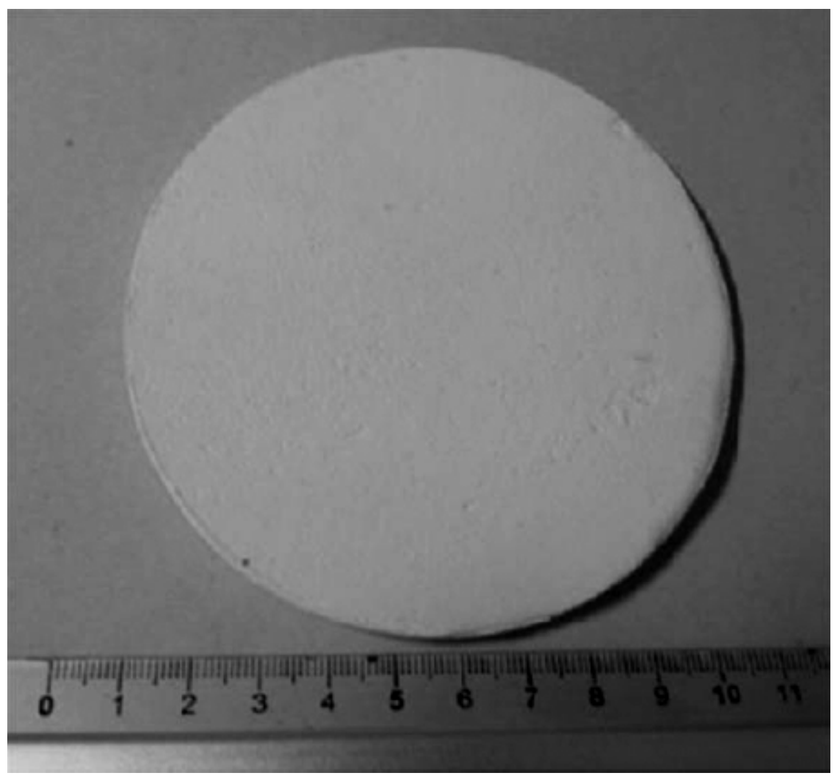

Fig. 4. YSZ target for magnetron sputtering.

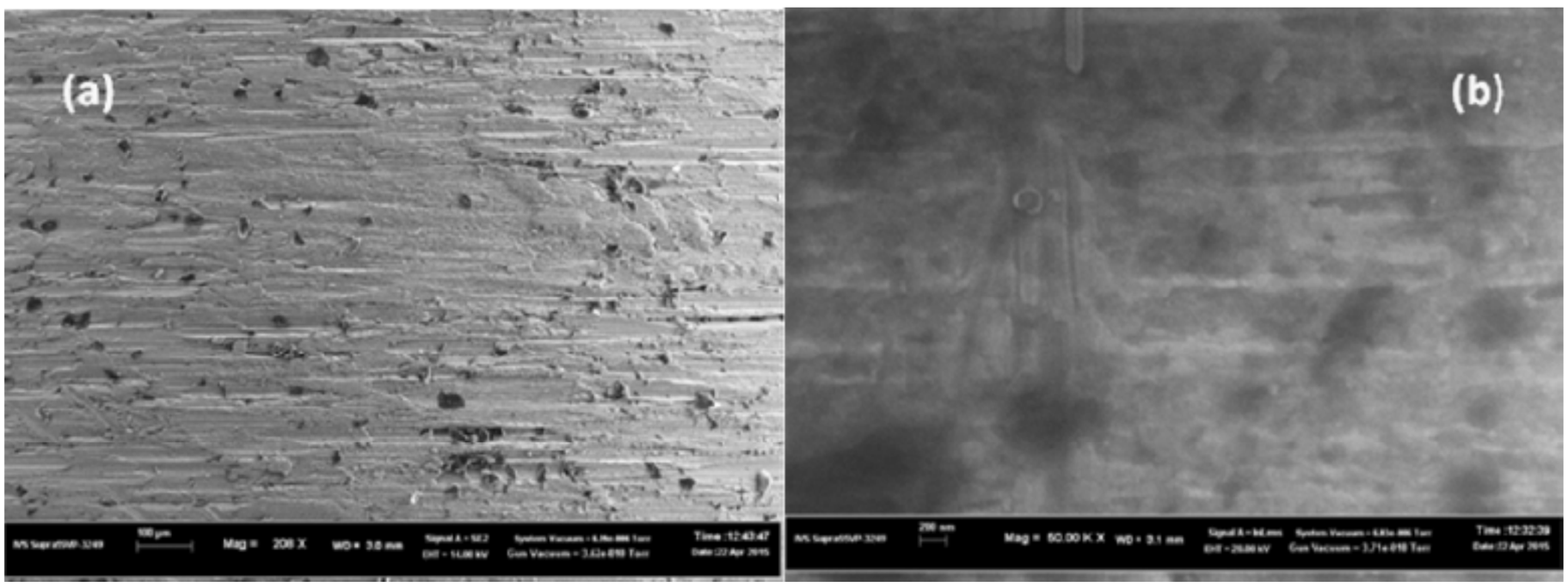

Fig. 5. Microstructure of YSZ coatings: (a) – 100 μm, (b) – 200 nm scale.

agglomerate size below 100 nm were produced. Table 2 presents the BET estimates of these values for various salt concentrations. Note that PSD analysis results in the same nanoscale sizes of particles in the precursor powders.

Then, thermogravimetric and XRD data were used to prove the fact that the above procedure provides the fluorite-like modification of precursor powders.

In order to produce the target for magnetron sputtering, precursor powders were compacted using a White spirit based binder (25 tons for 40 min); then dried till the complete binder elimination (110 °C), and annealed at 1550 °C in air for 1 hour. Fig. 4 presents the photo of the target.

Magnetron sputtering was performed using ASPIRA (ISOVAC Co., Belarus) installation, which includes RF magnetron with power supply (Stolberg HF GmbH, Germany) and built-in ion cleaning source. Both surface cleaning and sputtering were performed in Ar with its flow being 700-900 mL/min. The surface ion cleaning was carried out at residual pressure - 2.5 10^{-5} Pa, 1500 V, 70 mA for 400 sec. Magnetron sputtering was performed at 0.1 Pa under 600 V magnetron voltage and 1 kW power with the process duration ≈180-300 min.

As a result, quite uniform coatings with a high quality surface were produced on flat and cylindrical specimens of nanostructured titanium. The coating thickness obtained at 3 hr process duration was estimated as that ranging from 0.8 to 1.5 μm.

XRD data prove that the deposited YSZ coating is a mixture of fluorite-like, tetragonal, and monoclinic phases. However, fluorite-like phase that is preferable for practical applications seems to be dominant. X-ray fluorescence probe (INCA Microanalysis systems) was used to determine the coating chemical composition. The analysis of the obtained data shows that the deposited coating composition deviates from that of the target. In particular, yttrium oxide content in the coating is lower than 9 vol.%. However, it could be concluded that deposited coating has the YSZ composition with a constant Y-to-Zr ratio. This partial depletion in Yttria is likely due to the difference in the evaporation of corresponding oxides; we assume it as a source of minor content of tetragonal and monoclinic phases in the deposited coating.

Fig. 5 illustrates the structure of the YSZ-coated nanostructured Ti cylinder. This structure is quite uniform on the nanoscale level.

Note that magnetron sputtering is a rather complicated and expensive technique, and the duration of the deposition is relatively high. In this context, an alternative cost-effective approach was suggested to produce Ti-YSZ nanocomposites. The general idea was to create oxidized level on the Ti surface and to deposit YSZ using the method similar to that previously exploited for fabrication of the YSZ target.

Within the alternative approach, the following two YSZ compositions were utilized: $8Y_2O_3$-$91ZrO_2$ (as with the YSZ target) and $8Y_2O_3$-$10TiO_2$-$81ZrO_2$. The latter composition contains Ti oxide in order to increase the coating binding with the oxidized metal surface.

The deposition technique is briefly as follows. First, the procedure of sol-gel reverse precipitation was used. The oxidized titanium plate (standard VT0 Ti) was placed into the reaction volume just before the synthesis onset. The plate was removed from the reaction volume after the end of the synthesis and washed by distilled water until neutral wash water pH. Then, the plate was annealed at 550 °C for 5 hours in the air atmosphere. In another version, the resulted gel of mixed hydroxides was also washed until neutral pH, and oxidized Ti wafers were covered by a gel layer. The following freeze-drying at *P* = 0.018 atm. for 24 hours at -50 °C (Labconco,

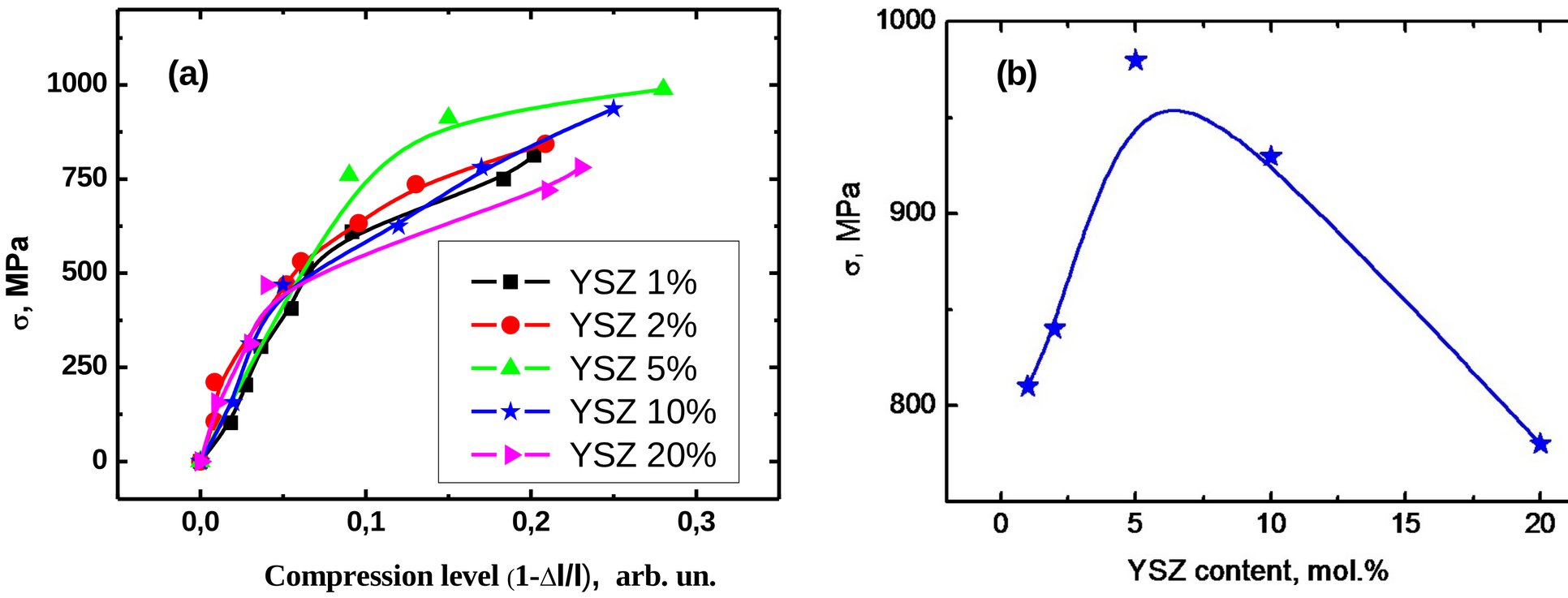

Fig. 6. Compressive strength data for nano Ni-YSZ composite: (a) set of experimental data; (b) compressive e strength limit.

Chamber 1L) was carried out. The last stage of this approach was annealing of the plate at 550 °C.

With SEM, XRD, and EDX studies, we revealed that the deposited layer is YSZ ceramics with the compositions listed above. High quality of this coating was proved with the reasonable level of coating-to-wafer binding. The results of mechanical tests (Brinell and Moos hardness determination) showed some enhancement in the mechanical properties of Ti plate coated by YSZ, as compared to those of pure Ti. In particular, Brinell hardness of the coated specimens was nearly 25% higher than that exhibited by pure Ti. Thus, one can conclude that the suggested technique to produce Ti-YSZ nanocomposites serves as a good alternative to magnetron sputtering. However, some problems with nano-Ti oxidation could come into play that need to be carefully examined in the future. More details on Ti-YSZ nanocomposites are presented in Refs. [23,24].

3.3. Ni-YSZ and Al-YSZ bulk nanocomposites

The YSZ ceramic phase with the $8Y_2O_3$-$92ZrO_2$ composition was taken to produce Ni-YSZ and Al-YSZ bulk nanocomposites. Fine Al-ASD and coarse Al-PA4 were utilized as initial metallic constituents in fabrication of Al-YSZ powders. Ni nanopowder (Advanced Powder Tech., Russia; average particle size ~75-80 nm) and coarse PNA-1 (average particle size < 20 μm) were taken as initial constituents of Ni-YSZ powders.

Let us briefly describe synthesis technique in the exemplary case of Ni-YSZ bulk nanocomposite. Coarse Ni powder was additionally meshed to eliminate large particles (>40 μm). Then, Ni-YSZ powder mixtures containing 1,2,3,5,10, and 20 wt.% YSZ were prepared. These mixtures were ball milled in a planetary mill (Pulverisette 6, 450 rpm, 3 min reverse cycle, 5 hours). Milled and mechanically activated powders were compacted into pellets (∅30 mm, height 15 mm) at 15 ton/cm^2 for 15 min, White spirit based binder was used. The drying at 110 °C removed the binder traces, and following annealing at 1250 °C in vacuum furnace was the final step of the synthesis. As a result, we obtained Ni-YSZ bulk nanocomposites.

XRD, SEM, and EBSD characterization indicates that YSZ inclusions in the composite bulk remain being in fluorite-like modification. Also, initial metal powder dispersity, synthesis procedure (annealing temperature) and YSZ content in final nanocomposite are revealed to exert pronounced effects on the microstructure. Several mechanical tests were performed demonstrating the effects of YSZ nanoinclusions on the mechanical properties exhibited by nanonickel-YSZ bulk nanocomposites (Fig. 6). More details on Ni-YSZ and Al-YSZ nanocomposites are presented in Refs. [25,26].

4. CONCLUSIONS

Thus, several new approaches are suggested and considered which are developed to fabricate novel metal (Al)–graphene and metal (Ti, Ni, Al)-YSZ ceramic nanocomposites with enhanced mechanical and other properties. In the framework of these approaches, it is possible to effectively tune and control both structural peculiarities and structure-sensitive properties of the nanocomposites. In the context discussed, this research reveals scientifically and practically interesting "fabrication-structure-properties" relationships in novel metal-graphene and

metal-ceramic nanocomposite materials, exploiting new approaches to their fabrication.

ACKNOWLEDGEMENTS

This work was supported by the Russian Science Foundation (Grant 14-29-00199).

REFERENCES

[1] A.K. Geim and K. S. Novoselov // *Nature Materials* **6** (2007) 183.
[2] F. Molitor, J. Guttinger, C. Stampfer, S. Droscher, A. Jacobson, T. Ihn and K. Ensslin // *Journal of Physics: Condensed Matter* **23** (2011) art. 24321.
[3] A.A. Balandin // *Nature Materials* **10** (2011) 569.
[4] I.A. Ovid'ko // *Reviews on Advanced Materials Science* **34** (2013) 1.
[5] C. Lee, X. Wei, J.W. Kysar and J. Hone // *Science* **321** (2008) 385.
[6] I.A. Ovid'ko // *Reviews on Advanced Materials Science* **38** (2014) 190.
[7] J. Wang, Z. Li, G. Fan, H. Pang, Z. Chen and D. Zhang // *Scripta Materialia* **66** (2012) 594.
[8] Z. Li, G.L. Fan, Z.Q. Tan, Q. Guo, D.B. Xiong, Y.S. Su, Z.Q. Li and D. Zhang // *Nanotechnology* **25** (2014) art. 325601.
[9] M. Rashad, F.S. Pan, A.T. Tang and M. Asif // *Progress in Natural Science: Materials International* **24** (2014) 101.
[10] S.F. Bartolucci, J. Paras, M.A. Rafiee, J. Rafiee, S. Lee, D. Kapoor and N. Koratkar // *Materials Science & Engineering A* **528** (2011) 7933.
[11] Y. Kim, J. Lee, M.S. Yeom, J.W. Shin, H. Kim, Y. Cui, J.W. Kysar, J. Hone, Y. Jung, S. Jeon and S.M. Han // *Nature Communications* **4** (2013) 2114.
[12] L. Mishnaevsky Jr, E. Levashov, R.Z. Valiev, J. Segurado, I. Sabirov and N. Enikeev // *Materials Science and Engineering R* **81** (2014) 1.
[13] C.C. Koch, I.A. Ovid'ko, S. Seal and S. Veprek, *Structural Nanocrystalline Materials: Fundamentals and Applications* (Cambridge: Cambridge University Press; 2007).
[14] R.Z. Valiev, A.P. Zhilyaev and T.G. Langdon. *Bulk Nanostructured Materials: Fundamentals and Applications* (Hoboken: Wiley; 2014).
[15] H. J. Wenz, J. Bartsch, S. Wolfart and M. Kern // *The International journal of prosthodontics* **21** (2007) 27.
[16] P. F. Manicone, P. R. Iommetti and L. Raffaelli // *Journal of dentistry* **35** (2007) 819.
[17] M. Hisbergues, S. Vendeville and P. Vendeville // *Journal of Biomedical Materials Research Part B: Applied Biomaterials* **88** (2009) 519.
[18] R.J. Kohal, D. Weng, M. Bahle and J.R.Strub // *Journal of Periodontology* **75** (2004) 1262.
[19] A.P. Zhilyaev, S.N. Sergeev, V.A. Popov and A.V. Orlov // *Reviews on Advanced Materials Science* **39** (2014) 15.
[20] A. Morales-Rodriguez, A. Bravo-Leon, A. Dominguez-Rodriguez, S. Lopez-Esteban, J.S. Moya and M. Jimenez-Melendo // *Journal of the European Ceramic Society* **23** (2003) 2849.
[21] C. Pecharromán, F. Esteban-Betegón, J.F. Bartolomé, G. Richter and J.S. Moya // *Nano Letters* **4** (2004) 747.
[22] V.G. Konakov, I.A. Ovid'ko, N.V. Borisova, E.N. Solovyeva, S.N. Golubev, O.Yu. Kurapova, N.N. Novik and I.Yu. Archakov // *Reviews on Advanced Materials Science* **39** (2014) 41.
[23] V.G. Konakov, I.A. Ovid'ko, O.Yu. Kurapova, N.N. Novik and I.Yu. Archakov // *Reviews on Advanced Materials Science* **41** (2015) 99.
[24] V.G. Konakov, O.Yu. Kurapova, N.N. Novik, M.M. Pivovarov and I.Yu. Archakov // *Reviews on Advanced Materials Science* **43** (2015) 94.
[25] V.G. Konakov, I.A. Ovid'ko, E.N. Solovyeva, O.Yu. Kurapova, N.N. Novik and M.M. Pivovarov // *Materials Physics and Mechanics* **24** (2015) 331.
[26] V.G. Konakov, E.N. Solovyeva, O.Yu. Kurapova, N.N. Novik, M.M. Pivovarov and I.Yu. Archakov // *Materials Physics and Mechanics* **24** (2015) 340.